RSC Advances

PAPER

View Article Online
View Journal | View Issue

Cite this: *RSC Adv.*, 2021, **11**, 2346

Atmospheric oxidation of Folpet initiated by OH radicals, NO_3 radicals, and O_3†

Chenxi Zhang, [ab] Xiaomin Sun, [b] Wei Tan[c] and Hengjun Peng*[d]

Received 5th November 2020
Accepted 30th December 2020

DOI: 10.1039/d0ra09429c

rsc.li/rsc-advances

Folpet, a nonspecific sulfenimide fungicide, is widely used to protect crops against mildew. It can be dispersed and transported over long distances. The residence time of Folpet in the atmosphere depends on the oxidation processes initiated by atmospheric oxidants such as O_3, OH and NO_3 radicals. In this study, the reactions of Folpet with gas-phase O_3, OH and NO_3 radicals were investigated *via* quantum chemical calculation methods, which can effectively provide information about the reaction intermediates and pathways. The obtained results show that the room-temperature rate constants of the reactions between Folpet and OH radicals, NO_3 radicals and O_3 are about 3.69×10^{-14}, 5.40×10^{-15}, and 1.73×10^{-22} cm^3 per molecule per s at 298 K, respectively. Considering the oxidant concentration in the atmosphere, Folpet seems to be mainly scavenged by NO_3 radicals, especially at night. This study can contribute to a better understanding of the atmospheric fate of Folpet, elucidating a significant impact of NO_3 radicals on its degradation process in comparison with other oxidants such as O_3 and OH radicals.

Introduction

Pesticides are widely used to kill pests and increase crop yields around the world. This inevitably leads to a release of environmental and foodborne contaminants, which has been shown to cause many diseases including cancer.[1] Thus the environmental fate of pesticides has become a hot topic. Up to 90% of pesticides applied in the agricultural field do not reach the target site, but end up being found in the soil, water and atmosphere.[2] It is worth noting that 30–50% of pesticides are transferred to the atmosphere *via* spray drift, evaporation, volatilization and windblown soil.[2–5]

Folpet (*N*-trichloromethyl-thio-phthalimide) is a nonspecific sulfenimide fungicide, which consists of a phthalimide moiety (PI) and a trichloromethylthio group ($SCCl_3$) (Fig. 1). Since 1952, Folpet has been widely employed on grapevines and other fruit trees to prevent diseases caused by mildew, grey mould, spoilage fungi and wood-decay fungi.[6,7] In addition, Folpet is also used as a raw material in the production of oil-based paints, coatings and plastics.[8]

Due to a low vapor pressure (2.1×10^{-5} Pa at 25 °C), Folpet is expected to found in both gas phases and particulate phases of the atmosphere. In general, the reported values are the sum of the pesticides present in both the gas and particulate phases, although some studies have separately reported the distribution in gases and particles. The air Folpet concentrations assessed in different places of the world range from pg to ng per m^3. A study by Raina *et al.* in the Lower Fraser Valley agricultural region of Canada reveals a maximum air Folpet total concentration of 1.7 ng m^{-3}.[9] The maximum Folpet total concentration detected by Coscollà *et al.* in the Central Region of France during a period of 2006–2008 was as high as 82.2 ng m^{-3}.[10] In turn, Folpet concentrations in the Centre of Reims (France), were reported to be not higher than 4.70 ng m^{-3}.[11] Furthermore, these assessed during sampling campaign by Schummer *et al.* varied from 0.39 to 11.3 ng m^{-3}, and Folpet was mostly present in the gas phase (about 68%).[12] Finally, high levels of PM_{10} Folpet concentrations from 11.4 to 162.0 pg m^{-3} were found within 24 hours of sampling in Spain.[13]

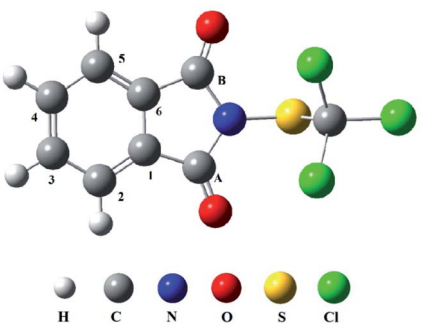

Fig. 1 The structure of Folpet.

[a]*College of Biological and Environmental Engineering, Binzhou University, Binzhou 256600, P. R.China*

[b]*Environment Research Institute, Shandong University, Qingdao 266200, P. R. China*

[c]*Shandong Provincial Eco-environment Monitoring Center, Jinan 250100, P. R. China*

[d]*Logistics Support Department, Shandong University, Jinan 250100, P. R. China. E-mail: phj@sdu.edu.cn*

† Electronic supplementary information (ESI) available. See DOI: 10.1039/d0ra09429c

Once in the atmosphere, the fate of pesticides is dictated by dry and wet deposition,[14] as well as by the chemical processes including photolysis and oxidation initiated by atmospheric oxidants such as O_3, OH, and NO_3 radicals.[15–20] Wet and dry deposition are physical removal processes and will not be removed from the environment. In turn, the efficiency of photolysis depends on three factors: absorption cross section, quantum yield for photo-induced reactions, and actinic flux of solar radiation. While the photon flux can be accurately calculated as a function of time of day, season and latitude, the measurement of absorption cross-sections and quantum yield can not presently be estimated.[21] Thus, photolysis rates can not be estimated reliably. Oxidation induced by atmospheric oxidants is expected to play a major role in the atmospheric chemistry of pesticides. In this respect, studying the mechanism and kinetics of atmospheric chemical reactions to understand the behavior of pesticides in the environment is an important task.

Earlier studies reveal that pesticides undergo oxidation reactions with atmospheric oxidants. Dang *et al.* investigated the atmospheric oxidation of *p*,*p*′-dicofol by OH and NO_3 radicals, and the rate constants for the reactions of *p*,*p*′-dicofol with OH and NO_3 radicals are 1.51×10^{-12} and 8.88×10^{-14} cm^3 per molecule per s, respectively.[22] El Masri *et al.* studied the kinetics and mechanism of heterogeneous oxidation of chlorpyrifos (CLP) and chlorpyrifos oxon (CLPO) by O_3 and OH radicals at room temperature using a photochemical reactor coupled to a GC/MS analytical system.[23] The result shown that the rate constants for the reactions of CLP and CLPO with O_3 are $(1.2 \pm 0.1)\times10^{-19}$ cm^3 per molecule per s and $(2.9 \pm 0.7)\times10^{-21}$ cm^3 per molecule per s, respectively. And the rate constants of CLP and CLPO with OH radical range between 6×10^{-12} and 2×10^{-14} cm^3 per molecule per s. There are also some pesticides with atmospheric oxidants has already been studied. But unfortunately, there are still a few studies concerning the degradation of Folpet by atmospheric oxidants.[24,25] To date, there are still a few studies concerning the degradation of Folpet by atmospheric oxidants. Among them, two works were dedicated to the determination of the kinetic rate constants for the reactions between Folpet, O_3 and OH radicals in the heterogeneous phase.[26,27] Their values were $(2.6 \pm 0.2) \times 10^{-20}$ cm^3 per molecule per s for the reaction induced by O_3 and $(1.6 \pm 0.9) \times 10^{-13}$ cm^3 per molecule per s in the case of the process involving the OH radical. Furthermore, it was shown that pesticide reactivity in the heterogeneous phase may be affected by the chemical properties of the supporting surface.[26] In this study, the degradation processes of the gas-phase Folpet with O_3, OH and NO_3 radicals were investigated *via* the quantum chemical calculation approaches, which can effectively provide information on the reaction intermediates and pathways. The rate constants of all initial pathways were then used to assess the fate and resistance of Folpet in the atmosphere.

Computational methods

Mechanism computations

All thermodynamics calculations were performed using Gaussian 09 software.[28] The geometrical parameters of reactants, intermediates, transition states (TS) and products in each elementary reaction were optimized by applying M06-2X functional with a standard 6-31+G(d,p) basis set. Zheng *et al.* has employed 348 model chemistries to calculate the 24 barrier heights in the DBH24/08 database, which including heavy-atom transfer (HATBH6), nucleophilic substitution (NSBH6), unimolecular and association (UABH6), and hydrogen-transfer (HTBH6) reactions.[29] The selected M06-2X/6-31+G(d,p) was proven to meet the need of both high accuracy and low computational cost. In this paper, TSs were examined by vibrational frequency analysis. A larger basis set, 6-311++g(3df,3pd), was used in the same method to obtain more accurate single energies.

Kinetics computations

Using the above calculated potential energy surface, the kinetics were obtained using KisThelP software based on the Transition State Theory (TST) with a Eckart tunneling correction factor.[30,31] The following thermodynamic equivalent is employed in KiSThelP:[32]

$$k^{\mathrm{TST}}(T) = \sigma \frac{k_b T}{h} \left(\frac{RT}{P^0}\right)^{\Delta n} e^{-\Delta G^{0,\neq}(T)/k_b T} \quad (1)$$

where σ is the reaction path degeneracy, k_b is the Boltzmann's constant, T is the temperature, h is the Planck's constant, RT/P^0 has units of inverse concentration (R is the ideal gas constant at $P^0 = 1$ bar), Δn is 1 or 0 for gas-phase bimolecular or unimolecular reactions, respectively, and $\Delta G^{0,\neq}(T)$ represents the standard Gibbs free energy of activation for the considered reaction. A scaling factor of 0.967 was imposed on the frequencies calculated at the M06-2X/6-31+G(d,p) level.[33]

Results and discussion

Reactions with OH radicals

Atmospheric OH radical mainly originates from the photolysis of ozone in the presence of water ($O(1D) + H_2O \rightarrow 2OH$).[34] It is often called the "detergent" of the troposphere: reacting with many organic compounds and pollutants, it decomposes them through "cracking", often acting as the first step to their removal. Furthermore, OH radical plays an important role in eliminating some greenhouse gases like methane and ozone, as well as inactivating pathogenic viruses and bacteria and neutralising allergenic pollens and mould spores. The reaction of the OH radical with an organic compound can be described by the two general processes: OH radical addition and H-atom abstraction.[35] For convenience, the atom number of Folpet is labeled in Fig. 1. As seen, a Folpet structure has four different carbon sites relative to the $-SCCl_3$ group, which can be attacked by OH radicals: the carbon atom of C=O (C_A, C_B), α-position carbon (C_α-C_1, C_6), β-position carbon (C_β-C_2, C_5), and λ-position carbon (C_λ-C_3, C_4). To avoid repetition, C_1, C_2 and C_3 positions were described in following article. H-atom abstraction will occur at the H atom linked with C_β and C_λ atoms. C_2 and C_3 positions were described as examples. The reaction pathways of OH radical addition and H atom abstraction are depicted in

Fig. 2. In this figure, the potential barriers (E_b) and the reaction heat (E_r) are marked as well. The optimized transition state structures of Folpet with OH radicals are shown in Fig. 3.

(A) OH radical addition pathways. OH radical addition to an aromatic ring can occur at C_1, C_2 and C_3 positions through three transition states, *i.e.*, TS1-1(OH), TS1-2(OH), and TS1-3(OH), respectively. The potential barriers for these processes are at the level of 3.30–4.25 kcal mol^{-1}. The distance between the OH radical and the C atom inside the transition state covers a range from 1.964 to 1.992 Å. All these processes are strongly exothermic, resulting in at least 9.06 kcal mol^{-1} of the energy released. Compared with addition reactions involving the aromatic rings, the OH radical added to C_A at the C=O bond generates IM1-A(OH) with a higher potential barrier (12.60 kcal mol^{-1}). The length of a newly formed C_A–O bond in TS1-A(OH) is 1.826 Å. This process is also exothermic, but the amount of energy released (4.68 kcal mol^{-1}) is less than that during the addition to the aromatic ring. Thus, OH radical addition to the aromatic ring is an energetically more favorable reaction pathway.

(B) H atom abstraction pathways. As seen in Fig. 2, due to its nucleophilicity, OH radical can abstract the H atoms at C_2 and C_3 positions, generating two intermediates (IM1-1′ and M1-2′) and H_2O. The potential barriers for these processes are 2.73 and 4.53 kcal mol^{-1}, respectively, which are comparable to the above described OH radical addition to the aromatic ring. What is more, these reactions are also exothermic, yielding the energies of 3.70 and 5.92 kcal mol^{-1}, which are inferior to the value associated with the addition reaction to the aromatic ring.

(C) Reaction rate calculations. The contributions of the six pathways during the reactions between Folpet and OH radicals were evaluated *via* the kinetics studies of the initial reaction. For this, reactions were simulated in a temperature range of 268–313 K (at a step of 5 K) using KisThelP software. The rate constant k of each reaction pathway and the branching ratio R at different temperatures are shown in Fig. 4. The rate constant of the overall OH radical addition reaction for a multichannel reaction of Folpet with the OH radical is denoted as k_{add}(OH).

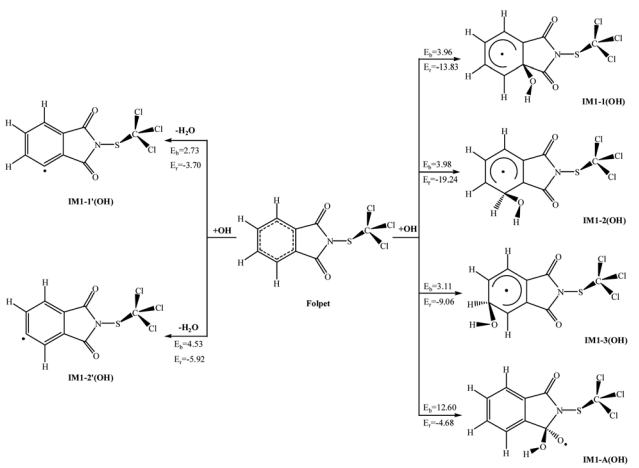

Fig. 2 The potential barriers E_b (kcal mol^{-1}) and reaction heats E_r (kcal mol^{-1}) at 298 K for the possible reactions of Folpet with OH radicals.

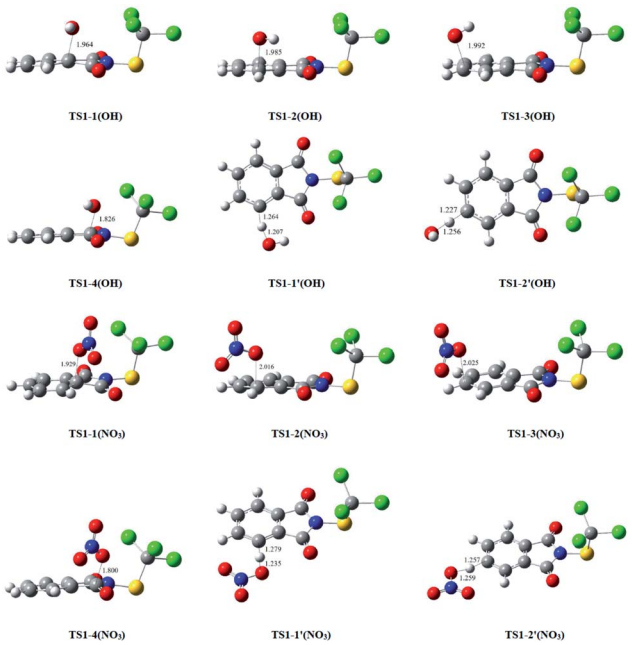

Fig. 3 The optimized transition state structures of Folpet with OH and NO_3 radicals.

The rate constant for the H-atom abstraction is referred to as k_{abs}(OH). The total rate constant for the reaction involving Folpet and OH radicals is k_{total}(OH), where k_{total}(OH) = k_{add}(OH)

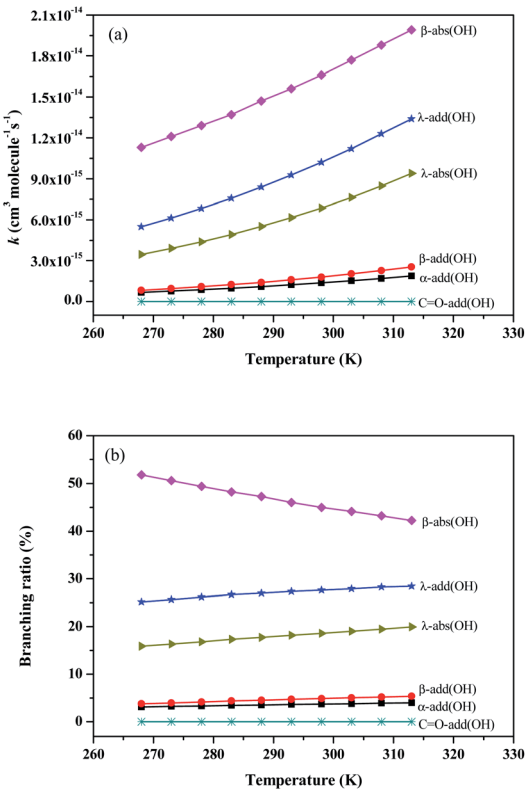

Fig. 4 The rate constants and branching ratios of the reaction of Folpet with OH radical at 268-313 K using the TST theory.

+ k_{abs}(OH). The branching ratio (R) for the ith entrance channel is determined as k_i(OH)/k_{total}(OH).

As seen in Fig. 4(a), the rate constants of α-add, β-add, λ-add, C=O-add, β-abs and λ-abs reactions are 1.38×10^{-15}, 1.80×10^{-15}, 1.02×10^{-14}, 1.48×10^{-21}, 1.66×10^{-14}, and 6.86×10^{-15} cm^3 per molecule per s at 298 K and 1 atm pressure, respectively. Since the rate constant of C=O-add reaction is much lower than others, this pathway is not dominant and can be negligible. The k_{add}(OH) and k_{abs}(OH) values are found to be 1.34×10^{-14} and 2.35×10^{-14} cm^3 per molecule per s, respectively, thus both OH radical addition reactions and H atom abstraction are important for Folpet. The k_{total}(OH) parameter is 3.69×10^{-14} cm^3 per molecule per s, which is slightly lower than that of $(1.6 \pm 0.9) \times 10^{-13}$ cm^3 per molecule per s in the heterogeneous phase.[27]

The branching ratio (R) can more intuitively express the contribution of each pathway. Fig. 4(b) shows the R values of all reaction pathways. Here, the dominant pathways are β-abs and λ-add, whose R values are around 47% and 27% within a studied temperature range. While the R value of β-abs pathway decreases from 51.8 to 42.3% with increasing temperature, that of λ-add rises from 25.2 to 28.5% within the above range of temperatures, implying that the increase of temperature is beneficial to λ-add pathway. As for other pathways, their degrees of contribution to the OH-initiated transformation of Folpet can be described by the following sequence: λ-abs > β-add > α-add > C=O-add.

Based on these results, it can be concluded that both OH radical addition and H-abstraction are important in the reactions between Folpet and OH radicals. Among them, β-abs is a dominant abstraction process, whereas the OH radical addition mainly acts on the C_λ sites.

Reactions with NO_3 radicals

The atmospheric NO_3 radical is derived from the reactions $NO + O_3 \rightarrow NO_2 + O_2$ and $NO_2 + O_3 \rightarrow NO_3 + O_2$.[36] Since this is a short-lived component with a lifetime of just about 5 s, its concentration remains low during the day, but it can be accumulated at night. Similar to the reactions with OH radicals, the NO_3 radical can be attached to the aromatic ring or the C=O bond, or can abstract an H atom from the C–H bond. The possible reactions of Folpet with NO_3 radicals are illustrated in Fig. 5, and the total rate constants (k) along with branching ratios (R) of each reaction site at 298 K are listed in Table 1.

According to data in Fig. 5, the addition reactions at the aromatic rings seem to be energetically favorable reaction pathways. These processes are exothermic, releasing energies of 4.60–12.46 kcal mol^{-1}, and possess low potential barriers (1.42–3.13 kcal mol^{-1}), being in contradiction to the reactions of OH radical addition and H atom abstraction that proceed with high activation barriers (E_b = 8.02–19.63 kcal mol^{-1}, E_r = 3.09–6.98 kcal mol^{-1}).

A comparative analysis of the k and R parameters at 298 K (Table 1) allows one to conclude that the rate constants for the addition reactions are much greater than those associated with the abstraction reactions, thus indicating a 100% contribution

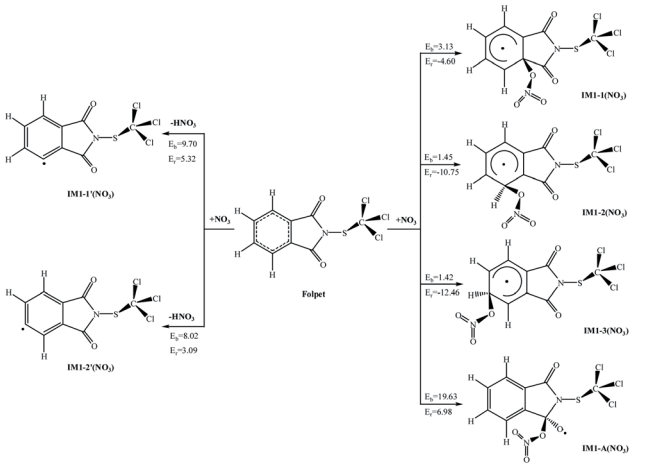

Fig. 5 The potential barriers E_b (kcal mol^{-1}) and reaction heats E_r (kcal mol^{-1}) at 298 K for the possible reactions of Folpet with NO_3 radicals.

Table 1 The total rate constants (k) and the branching ratios (R) at 298 K for each reaction site of Folpet with NO_3 radical

Reaction	$k_{298\ K}$ (cm^3 per molecule per s)	R (%)
Folpet + NO_3 → IM1-α(NO_3)	1.03×10^{-16}	1.9
Folpet + NO_3 → IM1-β(NO_3)	2.88×10^{-15}	53.3
Folpet + NO_3 → IM1-λ(NO_3)	2.42×10^{-15}	44.8
Folpet + NO_3 → IM1-C=O(NO_3)	4.19×10^{-28}	0
Folpet + NO_3 → IM1-β′(NO_3)	2.07×10^{-21}	0
Folpet + NO_3 → IM1-λ′(NO_3)	4.28×10^{-20}	0

of the addition reactions to the total process. The total rate constant is found to be 5.40×10^{-15} cm^3 per molecule per s, which is close to the values of reference compounds, such as 4.0×10^{-15} cm^3 per molecule per s of benzyl alcohol,[37] 6.8×10^{-14} cm^3 per molecule per s of dibenzo-*p*-dioxins,[38] and 9.3×10^{-15} cm^3 per molecule per s of dibenzofurans.[39]

Reactions with O_3 radicals

O_3 is a powerful oxidizing agent, which comes from eddy diffusion in the stratosphere or the photolysis of NO_2.[35,40] Unlike OH and NO_3 radicals, the reaction of O_3 with Folpet is only possible *via* the addition to the aromatic ring or the C=O bond, but never through the H-atom abstraction from a C–H bond. For O_3 added to Folpet, there are five eventual pathways (see Fig. 6).

According to the thermodynamic perspective, the addition to the aromatic ring is easier to occur than that to a C=O bond. In all the pathways, the addition of O_3 to C_2=C_3 and C_3=C_4 bonds results in the lowest barriers and the highest energies released. Table 2 show the total rate constants (k) and branching ratios (R) of each reaction site. The total rate constant of Folpet with O_3 is 1.73×10^{-22} cm^3 per molecule per s at 298 K, which is two orders of magnitude lower than that obtained in the heterogeneous phase.[26] As seen in Table 2, the addition reactions involving C_β=C_λ and C_3=C_4 bonds dominate over those with

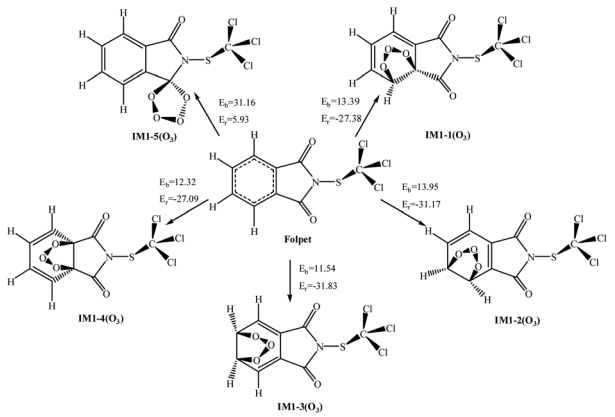

Fig. 6 The potential barriers E_b (kcal mol^{-1}) and reaction heats E_r (kcal mol^{-1}) at 298 K for the possible reactions of Folpet with O_3 radicals.

Table 2 The total rate constants (k) and the branching ratios (R) at 298 K for each reaction site of Folpet with O_3

Reaction site	$k_{298\ K}$ (cm^3 per molecule per s)	R (%)
C_α=C_β (O_3)	8.43×10^{-24}	5.0
C_β=C_λ (O_3)	5.25×10^{-23}	31.2
C_3=C_4 (O_3)	1.02×10^{-22}	59.9
C_1=C_6 (O_3)	6.59×10^{-24}	3.9
C=O (O_3)	4.22×10^{-34}	0

C_α=C_β and C_1=C_6 bonds within a studied temperature range. Consequently, the addition to a C=O bond can basically be ignored. It is worth noting that, while the branching ratios for the reactions with C_β=C_λ and C_3=C_4 bonds exhibit a slightly downward trend over the investigated temperature range, others are gradually rising.

The subsequent reactions of IM1-3(OH) and IM1-1′(OH)

In all the reactions, the OH radical addition to λ-site and H atom abstraction from β-site are most kinetically favored, thus IM1-3(OH) and IM1-1′(OH) are chosen as examples to illustrate the subsequent reaction in the atmosphere. The reaction paths are shown in Fig. 7 and 8, respectively.

(A) The fate of IM1-3(OH). In the atmosphere, IM1-3(OH) can be oxidized further by ubiquitous O_2. The O_2 addition to the π-delocalized electron systems of the IM1-3(OH) adducts occurs at both *ortho*-carbon atoms as well as the *para*-carbon of the C_3 position, producing peroxy radical isomers as depicted in Fig. 8. The potential barrier of the addition reactions ranges from 4.12 to 6.52 kcal mol^{-1}, and all the reactions are exothermic. Among them, the reaction barrier added to the *para*-carbon is the lowest and most likely to occur. Then the peroxy radical adduct IM2-2 can undergo further reaction *via* isomerization under low-NO_x conditions or reaction with NO under high-NO_x conditions.

Under low-NO_x conditions, the O atom of O_2 can attack the C atom of benzene ring to form five-member ring adduct (IM3-1 and IM3-2) or the four-member ring adduct (IM3-3 and IM3-

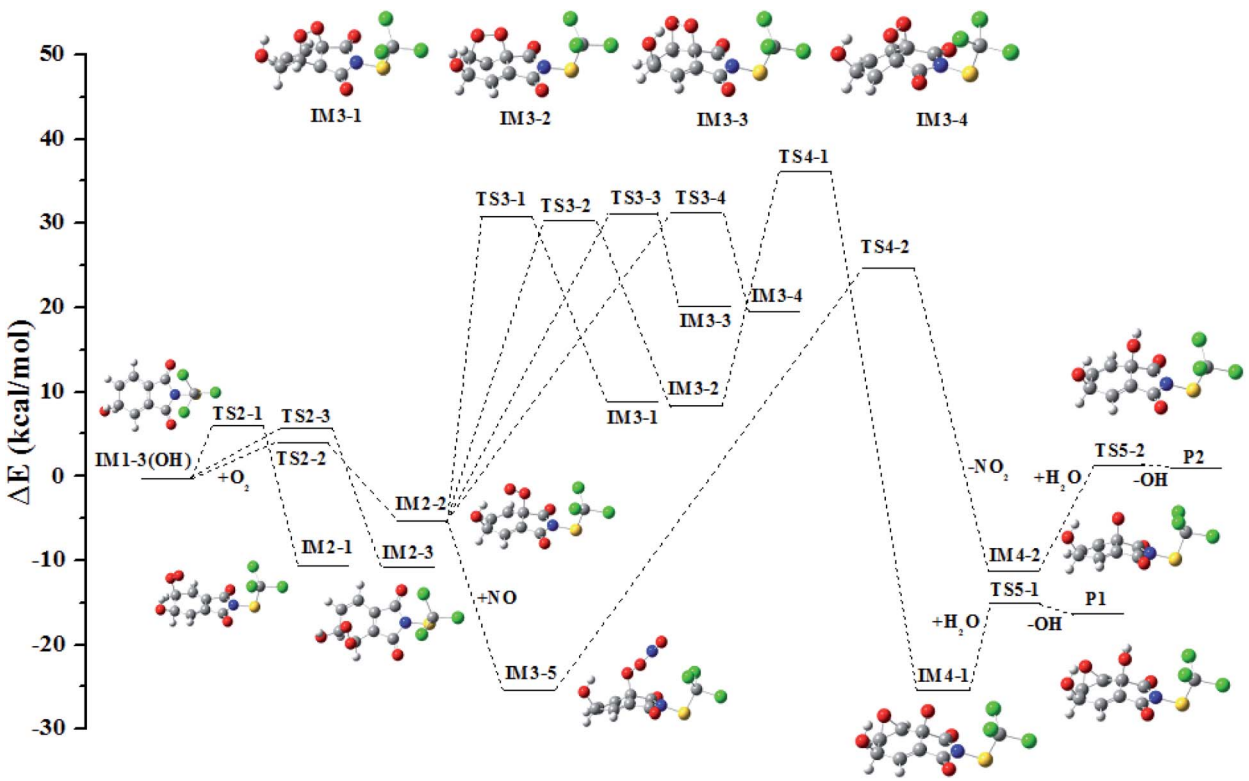

Fig. 7 The profile of the potential energy surface for the subsequent reactions of IM1-3(OH).

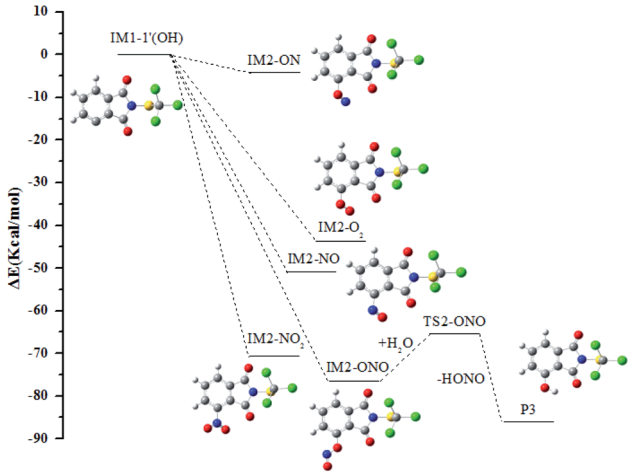

Fig. 8 The profile of the potential energy surface for the subsequent reactions of IM1-1′(OH).

4). All the isomerization reactions will pass through a high potential barrier and require heat absorption. Among them, the reaction forming IM3-2 has the lowest barrier. It will open up the O–O bond to form the intermediate IM4-1 subsequently. A three-member ring is formed simultaneously with the rupture of the O–O bond. The carbonyl free radical IM4-1 can abstract the H atom from H_2O to reach a stable state P1 and the OH radical will be regenerated simultaneously. The regenerated OH radical will initiate a new round of reaction.

Under high-NO_x conditions, it includes three elementary reactions: NO addition, NO_2 elimination, and reaction with H_2O. It should be pointed out that NO addition is a barrier-free combination and a strong exothermic process, resulting in an energy-rich intermediate that can be further reacted through unimolecular decomposition. The NO_2 elimination reaction has a high potential barrier of 51.35 kcal mol^{-1}, so it is the rate-determining mining step in the reaction path. The carbonyl free radicals IM4-2 can abstract the H atom in H_2O to regenerate OH radical and P2.

(B) The fate of IM1-1′(OH). IM1-1′(OH), as a radical, is quite active and can further react with O_2, NO and NO_2 in the atmosphere. Among them, NO and NO_2 can be added with O terminal or N terminal. The calculation results show that all reactions are barrierless. In all the reactions, the O-terminal addition reaction of NO_2 releases the most energy, up to 76.80 kcal mol^{-1}. The IM2-ONO can continue to react with H_2O to produce HONO and P3. The barrier of this reaction is 10.08 kcal mol^{-1}, it will release 10.14 kcal mol^{-1} of heat. The HONO is one of the main atmospheric sources of OH radicals which drive the chemistry of the troposphere.

The atmospheric lifetimes

The atmospheric lifetimes (τ) of Folpet corresponding to its reactions with highly reactive oxidants are defined by the formula: $\tau = 1/(k_x[X])$, where [X] is the atmospheric oxidant concentration. The concentration ranges of OH radical, NO_3 radical and O_3 are 3.5×10^5 to 2.00×10^6, 3×10^7 to 9×10^8 and 4.67×10^{11} to 1.17×10^{12} molecules per cm^3, respectively.[40–42] Using the above determined rate constants k, the lifetimes of Folpet with respect to O_3 is hundreds of years (159.2–398.9 years) in comparison to 5.2–29.8 months and 2.38 days to 2.38 months against OH radical and NO_3 radical. If the average concentration of OH radicals for 12 h daytime (1.6×10^6 molecule cm^3)[43] and the average concentration of NO_3 radicals for 12 h nighttime (1.1×10^8 molecule cm^3)[42] are used, the lifetime of about 6.5 months and 19.5 days are obtained, which shows that Folpet is relatively persistent towards oxidation removal processes.

Conclusions

The atmospheric oxidation mechanisms and kinetic phenomena arising in the reactions of Folpet with OH radicals, NO_3 radicals and O_3 were investigated using the DFT method. Two general reaction mechanisms were used to describe the above processes: (1) addition to the aromatic rings and C=O bonds, initiated by the OH radicals, NO_3 radicals and O_3 and (2) H-abstraction from C–H bonds, induced by OH and NO_3 radicals. While both the addition and H-abstraction were shown to be important for the OH radical-initiated reactions, the addition to the aromatic ring was found to dominate over the H-abstraction in the case of processes with NO_3 radicals. The room-temperature rate constants of the reactions involving OH radicals, NO_3 radicals and O_3 were about 3.69×10^{-14}, 5.40×10^{-15}, and 1.73×10^{-22} cm^3 per molecule per s, respectively. Considering the atmospheric oxidant concentrations, Folpet was shown to be mainly scavenged by NO_3 radicals, especially at night time.

Conflicts of interest

There are no conflicts to declare.

Acknowledgements

This work is supported by National Natural Science Foundation of China (21607011 and 21976109), Key Research and Development Project of Shandong Province (2019GSF109021 and 2019GSF109037), Natural Science Foundation of Shandong Province (ZR2018MB043), the Fundamental Research Funds of Shandong University (2018JC027).

References

1 E. S. O'Leary, J. E. Vena, J. L. Freudenheim and J. Brasure, *Environ. Res.*, 2004, **94**, 134–144.
2 Y. Gil and C. Sinfort, *Atmos. Environ.*, 2005, **39**, 5183–5193.
3 F. Van Den Berg, R. Kubiak, W. G. Benjey, M. S. Majewski, S. R. Yates, G. L. Reeves, J. H. Smelt and A. M. Van Der Linden, *Water, Air, Soil Pollut.*, 1999, **115**, 195–218.
4 O. Zivan, Y. Bohbot-Raviv and Y. Dubowski, *Chemosphere*, 2017, **177**, 303–310.
5 O. Zivan, M. Segal-Rosenheimer and Y. Dubowski, *Atmos. Environ.*, 2016, **127**, 155–162.

6 H. Teisseire and G. Vernet, *Pestic. Biochem. Physiol.*, 2001, **69**, 112–117.
7 J. F. Huertas-Pérez, M. Ernest, J. Varela and F. Badoud, *Food Chem.*, 2018, **260**, 213–220.
8 K. Chen, J. C. Mackie, E. M. Kennedy and B. Z. Dlugogorski, *Environ. Sci. Technol.*, 2011, **452**, 554–560.
9 R. Raina, W. Belzer and K. Jones, *Water, Air, Soil Pollut.*, 2009, **2**, 41–49.
10 C. Coscollà, P. Colin, A. Yahyaoui, O. Petrique, V. Yusà, A. Mellouki and A. Pastor, *Atmos. Environ.*, 2010, 3915–3925.
11 A. Villiot, E. Chrétien, E. Drab-Sommesous, E. Rivière, A. Chakir and E. Roth, *Atmos. Environ.*, 2018, **174**, 82–91.
12 C. Schummer, E. Mothiron, B. M. R. Appenzeller, A. Rizet, R. Wennig and M. Millet, *Environ. Pollut.*, 2010, **158**, 576–584.
13 E. Hart, C. Coscollà, A. Pastor and V. Yusà, *Atmos. Environ.*, 2012, **62**, 118–129.
14 M. S. Majewski, R. H. Coupe, W. T. Foreman and P. D. Capel, *Environ. Toxicol. Chem.*, 2014, **33**, 1283–1293.
15 R. Atkinson, R. Guicherit, R. A. Hites, W. U. Palm, J. N. Seiber and P. de Voogt, *Water, Air, Soil Pollut.*, 1999, **115**, 219–243.
16 E. Borras, M. Rodenas, T. Vera, T. Gomez and A. Munoz, *Sci. Total Environ.*, 2017, **579**, 1–9.
17 J. Socorro, P. S. J. Lakey, L. Han, T. Berkemeier, G. Lammel, C. Zetzsch, U. Poeschl and M. Shiraiwa, *Environ. Sci. Technol.*, 2017, **51**, 13749–13754.
18 W. H. Wang, K. Z. Aregahegn, S. T. Andersen, A. Z. Ni, A. F. Rohrbacher, O. J. Nielsen and B. J. Finlayson-Pitts, *J. Agric. Food Chem.*, 2019, **67**, 1638–1646.
19 C. Mattei, H. Wortham and E. Quivet, *Atmos. Environ.*, 2019, **211**, 170–180.
20 C. Mattei, H. Wortham and E. Quivet, *Sci. Total Environ.*, 2018, **625**, 1544–1553.
21 R. Atkinson, R. Guicherit and R. A. Hites, *Water, Air, Soil Pollut.*, 1999, **115**, 219–243.
22 J. Dang, S. Tian and Q. Z. Zhang, *Chemosphere*, 2018, **219**, 645–654.
23 A. El Masri, M. Al Rashidi, H. Laversin, A. Chakir and E. Roth, *RSC Adv.*, 2014, **4**, 24786–24795.
24 O. Rokbani, S. Fattouch, A. Chakir and E. Roth, *Sci. Total Environ.*, 2018, **694**, 133745.
25 T. Vera, E. Borras, J. M. Chen, C. Coscolla, V. Daele, A. Mellouki, M. Rodenas, H. Sidebottom, X. M. Sun and V. Yusa, *Chemosphere*, 2015, **138**, 112–119.
26 M. Al Rashidi, A. Chakir and E. Roth, *J. Phys. Chem. A*, 2013, **117**, 2908–2915.
27 M. Al Rashidi, A. Chakir and E. Roth, *Atmos. Environ.*, 2014, **82**, 164–171.
28 M. J. Frisch, G. W. Trucks, H. B. Schlegel and G. E. Scuseria, *et al.*, *Gaussian 09, revision D.01*, Gaussian, Inc., Wallingford, CT, 2009.
29 J. J. Zheng, Y. Zhao and D. G. Truhlar, *J. Chem. Theory Comput.*, 2009, **5**, 808–821.
30 C. Eckart, *Phys. Rev.*, 1930, **35**, 1303–1309.
31 H. Eyring, *Chem. Rev.*, 1935, **17**, 65–77.
32 S. Canneaux, F. Bohr and E. Henon, *J. Comput. Chem.*, 2014, **35**, 82–93.
33 I. M. Alecu, J. Zheng, Y. Zhao and D. G. Truhlar, *J. Chem. Theory Comput.*, 2010, **6**, 2872–2887.
34 R. Guicherit and M. Roemer, *Chemosphere: Global Change Sci.*, 2000, **2**, 167–183.
35 R. Atkinson and J. Arey, *Atmos. Environ.*, 2003, **37**, S197–S219.
36 R. Atkinson, D. L. Baulch, R. A. Cox, J. R. F. Hampson and J. Troe, *J. Phys. Chem. Ref. Data*, 1997, **26**, 1329–1499.
37 J. C. Harrison and J. R. Wells, *Int. J. Chem. Kinet.*, 2012, **44**, 778–788.
38 E. S. C. Kwok, R. Atkinson and J. Arey, *Int. J. Chem. Kinet.*, 1994, **26**, 511–525.
39 R. Atkinson, *Environ. Sci. Technol.*, 1996, **6**, 53–72.
40 J. A. Logan, *J. Geophys. Res.*, 1985, **90**, 10463–10482.
41 M. G. Lawrence, P. Jockel and R. von Kuhlmann, *Atmos. Chem. Phys.*, 2001, **1**, 37–49.
42 M. Vrekoussis, M. Kanakidou, N. Mihalopoulos, P. J. Crutzen, J. Lelieveld, D. Perner, H. Berresheim and E. Baboukas, *Atmos. Chem. Phys.*, 2004, **4**, 169–182.
43 R. Prinn, D. Cunnold, P. Simmonds, F. Alyea, R. Boldi, A. Crawford, P. Fraser, D. Gutzler and D. R. Rosen, *J. Geophys. Res.*, 1992, **97**, 2445–2461.